CHEMICAL PHYSICS

# Crystal nucleation initiated by transient ion-surface interactions at aerosol interfaces

Ryan D. Davis[1,2]* and Margaret A. Tolbert[1,2]†



**Particle collisions are a common occurrence in the atmosphere, but no empirical observations exist to fully predict the potential effects of these collisions on air quality and climate projections. The current consensus of heterogeneous crystal nucleation pathways relevant to the atmosphere dictates that collisions with amorphous particles have no effect on the crystallization relative humidity (RH) of aqueous inorganic aerosols because there is no stabilizing ion-surface interaction to facilitate the formation of crystal nuclei. In contrast to this view of heterogeneous nucleation, we report laboratory observations demonstrating that collisions with hydrophobic amorphous organic aerosols induced crystallization of aqueous inorganic microdroplets at high RH, the effect of which was correlated with destabilizing water-mediated ion-specific surface interactions. These same organic aerosols did not induce crystallization once internally mixed in the droplet, pointing toward a previously unconsidered transient ion-specific crystal nucleation pathway that can promote aerosol crystallization via particle collisions.**

## INTRODUCTION

Aqueous inorganic ions are a major component of atmospheric aerosols, typically comprising 25 to 75% of the dry aerosol mass (*1*, *2*), with the potential for enhanced concentrations of certain aqueous ions at the air-aerosol interface (*3*–*5*). At sufficiently low relative humidity (RH), aqueous inorganic aerosols can undergo crystallization with the loss of particle-phase water (efflorescence), which alters the aerosol's effect on global climate (*1*, *6*–*9*) and many heterogeneous and photochemical reactions that influence air quality and thus affect public health (*10*, *11*). Because of the importance of the aerosol phase, the efflorescence behavior of aqueous inorganic aerosols has been studied for decades and is thought to be well understood. However, there is no agreement on how crystals nucleate and grow from an aqueous solution (*12*–*15*), and empirical observations remain a necessity, as evident in recent laboratory and field studies that have revealed unexpected efflorescence behavior when particles collide (contact efflorescence) (*7*) and in mixed-phase aerosols (*6*). In particular, the effect of collisions on particle phase remains largely unexplored.

Insoluble amorphous particles, such as soot or organic colloids, can become internally mixed with aqueous aerosols via particle collisions (coagulation) (*7*–*9*, *16*–*18*). These particles are not expected to be effective heterogeneous nuclei because they do not contain a regular array of atoms or ions to help orient crystal lattice structure (*1*). Furthermore, some of the most abundant atmospherically relevant ions (for example, $Na^+$, $Cl^-$, and $SO_4^{2-}$) do not readily adsorb to hydrophobic surfaces (*3*, *4*, *19*–*22*). Many colloidal particles therefore lack the ability to organize these nonadsorbing aqueous ions into a well-organized crystal nucleus and initiate efflorescence, consistent with experimental observations (*8*, *9*). However, some ions (for example, $Br^-$ and $I^-$) do adsorb to a hydrophobic surface (*3*), and colloidal surfaces are known to strongly influence the interfacial composition and structure of aqueous phases via ion-surface, ion-water, and water-surface interactions (for example, Hofmeister effects) (*19*–*22*).

Our previous study involving collisions between aqueous droplets and soluble crystalline contact nuclei (CN) demonstrated that a nonequilibrium CN-droplet interface can persist long enough for crystal nucleation to occur epitaxially (that is, oriented by CN crystal lattice structure), although CN dissolution was predicted from bulk thermodynamics. The question arises whether these nonequilibrium effects may exist for collisions with other CN particle types, such as insoluble amorphous colloids, particularly considering the complexity of the ion-specific interfacial dynamics at the surfaces of these particles and the growing recognition of ion-specific and nonclassical crystal nucleation pathways (*14*, *19*).

Motivated by the atmospheric occurrence of coagulation involving a wide range of particle types (for example, soot and tar balls), we studied the effect of collisions between aqueous inorganic microdroplets and insoluble (hydrophobic) amorphous organic aerosols. Experiments were performed using optically levitated microdroplets of sodium chloride (NaCl), ammonium chloride ($NH_4Cl$), and sodium bromide (NaBr), which are important components of sea spray aerosol. In our optical levitation system, light-absorbing particles, such as soot, strongly absorb the trapping laser wavelength. Thus, to avoid these complications and to probe the potential relevance of ion-specific interactions on salt crystal nucleation, functionalized surfactant-free polystyrene latex spheres (PSLs), which are hydrophobic amorphous (glassy) organic aerosols, with a range of surface functionality/net charge were used as CN proxies for atmospherically relevant insoluble organic aerosols.

## RESULTS

### Efflorescence was observed in situ

Collision-induced (contact) efflorescence was studied for aqueous droplets of each salt with two different types of PSL CN. Experiments were also performed for droplets with internally mixed PSLs (internally mixed efflorescence) and for pure droplets (homogeneous efflorescence). These different modes of efflorescence are illustrated in Fig. 1. For all efflorescence experiments, a single aqueous droplet (~10 ± 2 μm in diameter) was optically levitated in a humidity-controlled flow cell (fig. S1) at a constant RH for a maximum residence time (τ) of 5 min. If no efflorescence was observed within τ, the droplet was ejected and the experiment was repeated with a fresh droplet. For internally mixed efflorescence, droplets were generated with an average of four

[1]Cooperative Institute for Research in Environmental Sciences, University of Colorado, Boulder, Boulder, CO 80309, USA. [2]Department of Chemistry and Biochemistry, University of Colorado, Boulder, Boulder, CO 80309, USA.
*Present address: Lawrence Berkeley National Laboratory, Berkeley, CA 94720, USA.
†Corresponding author. Email: tolbert@colorado.edu

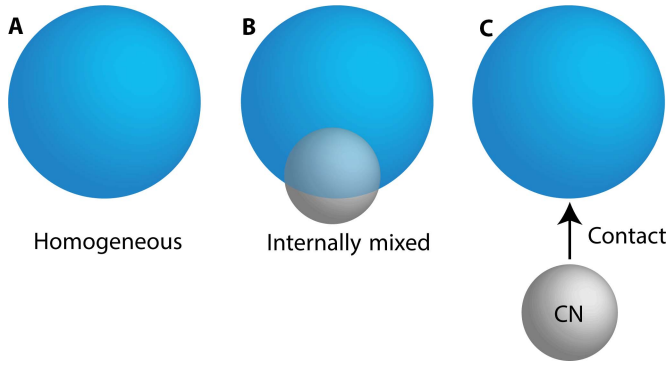


**Fig. 1. The modes of efflorescence of aqueous droplets studied here.** (**A**) Homogeneous efflorescence, that is, an aqueous droplet in the absence of any foreign surface; (**B**) internally mixed efflorescence, where PSLs are internally mixed in the aqueous droplet; and (**C**) collision-induced contact efflorescence, where a PSL CN makes external contact with an aqueous droplet.

premixed PSLs. For contact efflorescence experiments, a levitated droplet was exposed to a stream of PSL CN, and the occurrence of efflorescence and the number of CN-droplet collisions were directly quantified by imaging scattered laser light (see fig. S2 and movies S1 to S4) (*7*, *23*). The maximum number of collisions for a single droplet was 10. The CN types were amidine ($NHNH_2/NH_2NH_2^+$)–functionalized PSLs [(+)PSL; 400 nm in diameter] and carboxyl ($COOH/COO^-$)–functionalized PSLs [(−)PSL; 400 nm in diameter], which have a net positive and negative surface potential, respectively (table S1). Collision velocities were atmospherically relevant (~2 to 3 mm/s) (*7*). Bright-field images were also captured during some trials to verify our interpretation of the laser scatter images.

For statistical analysis, individual droplets were grouped into RH bins of ~1 to 3% RH, and the probability of homogeneous ($P_{hom}$) or internally mixed ($P_{IM}$) efflorescence was calculated as

$$P_{hom} \text{ and } P_{IM} = \frac{N_{eff}}{N_{tot}} \quad (1)$$

where $N_{tot}$ is the total number of ensemble droplets within the RH range and $N_{eff}$ is the number of those droplets that effloresced within $\tau$ (*8*). The probability of contact efflorescence ($P_{CE}$) was calculated as

$$P_{CE} = \frac{N_{eff}}{N_{col}} \quad (2)$$

where $N_{eff}$ is the number of ensemble droplets that effloresced upon a collision and $N_{col}$ is the total number of collisions observed, including the ones that did not induce efflorescence (*24*). The RH where $P_{hom}$, $P_{IM}$, and $P_{CE}$ = 0.5 was taken as the median efflorescence RH values $RH_{0.5}^{hom}$, $RH_{0.5}^{IM}$, and $RH_{0.5}^{CE}$, respectively. The effect of collisions relative to deliquescence and homogeneous efflorescence was quantified with the parameter $\sigma_{0.5}^{RH}$, given as

$$\sigma_{0.5}^{RH} = \frac{DRH - RH_{0.5}^{CE}}{DRH - RH_{0.5}^{hom}} \quad (3)$$

where DRH is the deliquescence RH of NaCl, $NH_4Cl$, or NaBr [75, 77, and 48% RH, respectively (*1*, *23*)]. $\sigma_{0.5}^{RH}$ has potential values between 0 and ~1, where $\sigma_{0.5}^{RH}$ = 0 corresponds to efflorescence at the DRH (that is, no supersaturation).

## Internally mixed PSLs did not induce efflorescence

The efflorescence results are summarized in Fig. 2 (A to C) (see tables S2 to S5 for results from individual experiments). The $RH_{0.5}^{hom}$ values for NaCl, $NH_4Cl$, and NaBr were 47 ± 1, 45 ± 1, and 26 ± 1% RH, respectively, consistent with literature values (*1*, *23*). The $RH_{0.5}^{IM}$ values for droplets with internally mixed PSLs were equivalent to $RH_{0.5}^{hom}$ for all salts. For NaCl and $NH_4Cl$, $P_{hom} \approx P_{IM}$ for all RH bins, demonstrating that PSLs do not serve as sites for heterogeneous nucleation of these two salts. Internally mixed PSLs appeared to remain in static contact with the droplet surface forming a three-phase interface (fig. S3), but no enhancement in crystal nucleation was observed. For NaBr with internally mixed PSLs, $P_{IM}$ was nonzero (≤0.3) up to ~36 to 40% RH, suggesting that PSLs may have a moderate effect on NaBr efflorescence. However, $P_{IM}$ remained low until ~27% RH, similar to the homogeneous case.

## Collisions with PSLs induced efflorescence at elevated RH

In stark contrast to the internally mixed efflorescence results, it can be seen that in all cases, collisions with PSL CN induced contact efflorescence at an elevated RH relative to homogeneous efflorescence. For a particular CN-droplet combination, the range of contact efflorescence RH values was dependent not only on the aqueous composition but also on the PSL CN surface functionality/charge, as evident in Fig. 2. With (−)PSL CN, $RH_{0.5}^{CE}$ was markedly high for NaCl and NaBr (63 ± 2 and 41 ± 2%, respectively). The effect of collisions with (−)PSL CN was less pronounced for $NH_4Cl$ ($RH_{0.5}^{CE}$ = 50 ± 2%) than for NaCl and NaBr. For $NH_4Cl$, collisions with (+)PSL CN had the largest effect ($RH_{0.5}^{CE}$ = 59 ± 2%). In contrast, with (+)PSL CN, $RH_{0.5}^{CE}$ shifted to lower values for NaCl and NaBr (57 ± 2 and 28 ± 2%, respectively). In all cases, the impact velocity and CN diameter were the same, suggesting that efflorescence was not induced because of a purely kinetic or mechanical effect [a supposition that was validated with 800-nm-diameter (−)PSL CN; see Supplementary Text]. Rather, the greatly different $RH_{0.5}^{CE}$ values for the various PSL-droplet combinations are indicative of ion-specific interactions between the aqueous ions and the PSL CN surface.

## Contact efflorescence RH is correlated with ion-surface interactions

Ion-surface interactions are a complex interplay of direct electrostatic and hydration-mediated interactions, which can lead to ion-specific accumulation/exclusion at a wide range of aqueous interfaces (*3*–*5*, *19*–*22*). In particular, both the long-range electrostatic attraction of the aqueous counterions to the charged PSL surface and the short-range hydration of those ions can strongly influence the PSL-droplet interfacial structure and composition, as illustrated in Fig. 2 (D to F) (*19*–*22*). Figure 2 suggests that the variation in the relative effect of collisions (that is, $\sigma_{0.5}^{RH}$) is correlated to the aqueous counterion attracted to the PSL surface. $\sigma_{0.5}^{RH}$ is similar for NaBr and NaCl with (−)PSL CN ($Na^+$ counterion) and also for NaCl and $NH_4Cl$ with (+)PSL CN ($Cl^-$ counterion). This would seem to suggest that the charged functional groups are facilitating template-directed crystal nucleation (*12*). However, the same effect would be expected with internally mixed PSLs, which was not the case here (except for a potential effect on NaBr efflorescence). It is thus necessary to also consider other ion-surface interactions.

Although functionalized, the PSL surfaces were predominately hydrophobic. The hydrophobic surface propensities of the ions in this

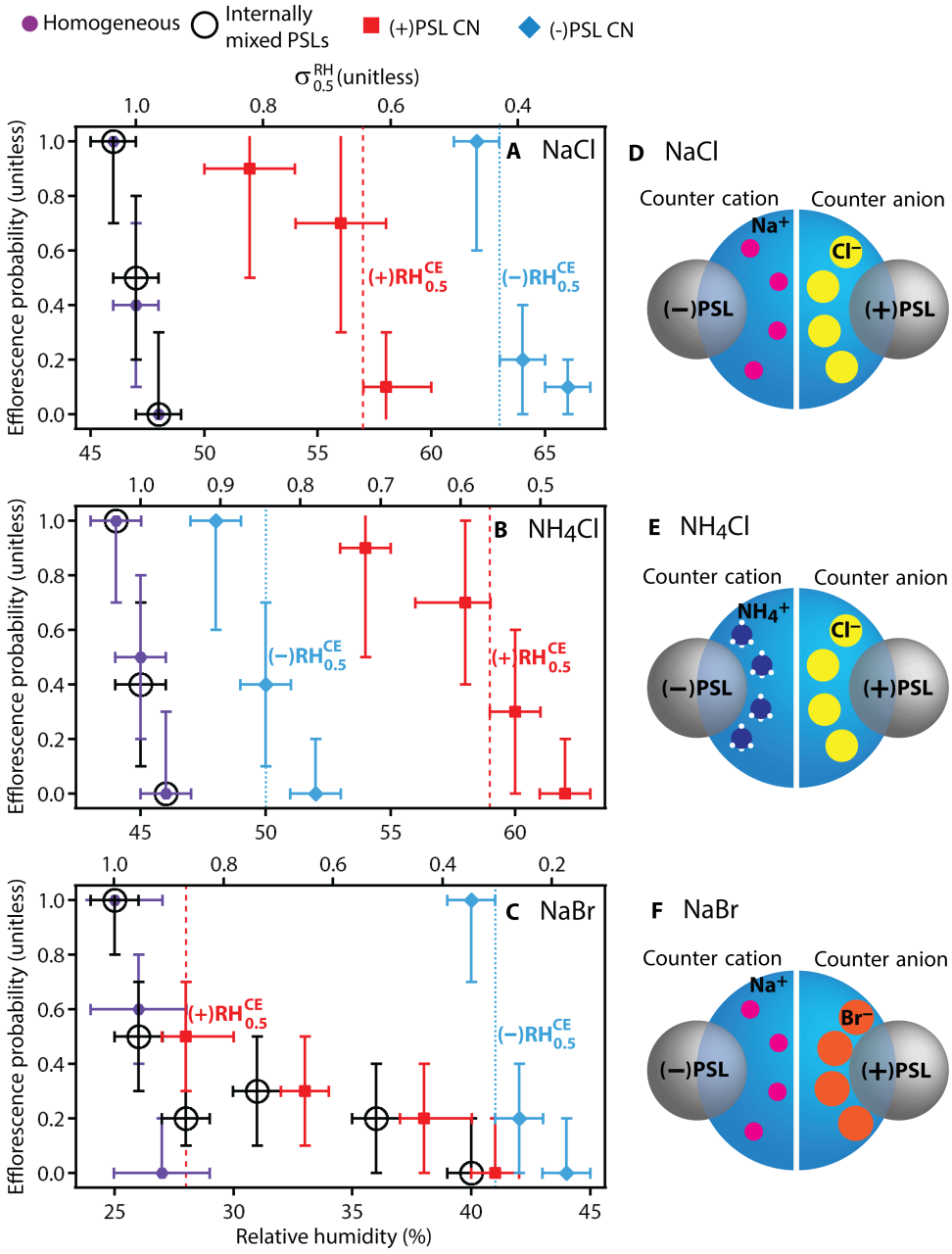


**Fig. 2. Efflorescence results and illustrated representations of the aqueous counterions.** (**A** to **C**) Efflorescence probability for homogeneous efflorescence, internally mixed PSL efflorescence, and contact efflorescence with PSL CN for aqueous NaCl (A), $NH_4Cl$ (B), and NaBr (C). Uncertainty in RH is the upper and lower quartiles of the RH bins. Uncertainty in $P_{hom}$ and $P_{IM}$ is $\pm 1/\sqrt{N_{tot}}$, and uncertainty in $P_{CE}$ is $\pm 1/\sqrt{N_{col}}$. $RH_{0.5}^{CE}$ values and their respective $\sigma_{0.5}^{RH}$ are indicated by the vertical dashed lines. (**D** to **F**) Illustrated representations of the aqueous counterions attracted to the carboxyl (–) and amidine (+) PSL CN surface groups. The spacing between the counterions and the PSL CN surface illustrates the relative surface propensity of the counterions. For clarity, the co-ions are not shown.

study follow the trend $NH_4^+ > Na^+$ for the cations and $Br^- > Cl^-$ for the anions; that is, $NH_4^+$ and $Br^-$ (weakly hydrated chaotropes) are able to more effectively approach a hydrophobic surface than $Na^+$ and $Cl^-$ (strongly hydrated kosmotropes) (*3*–*5*, *20*, *21*). As seen in Fig. 3A, when considering the hydrophobic surface propensity/hydration strength of the counterion (that is, Hofmeister effects), the results follow a trend where the decreasing surface propensity of the PSL counterion (that is, stronger repulsion from a hydrophobic surface) is correlated with a decrease in $\sigma_{0.5}^{RH}$ (increase in $RH_{0.5}^{CE}$). This trend is also reflected in ion-specific hydration properties, such as solvation free energy and Jones-Dole coefficient (a measure of ion-solute interaction strength), as seen in Fig. 3 (B and C, respectively). The lowest $\sigma_{0.5}^{RH}$ (highest $RH_{0.5}^{CE}$) was observed for $Na^+$, yet colloidal studies have suggested that this ion does not adsorb to negatively charged hydrophobic PSL surfaces (*21*), preferring to remain well hydrated away from the hydrophobic surface. This suggests that destabilizing hydration-mediated ion-surface interactions may be facilitating crystal nucleation upon contact, which would be in contrast to the prevailing theories of heterogeneous nucleation, which

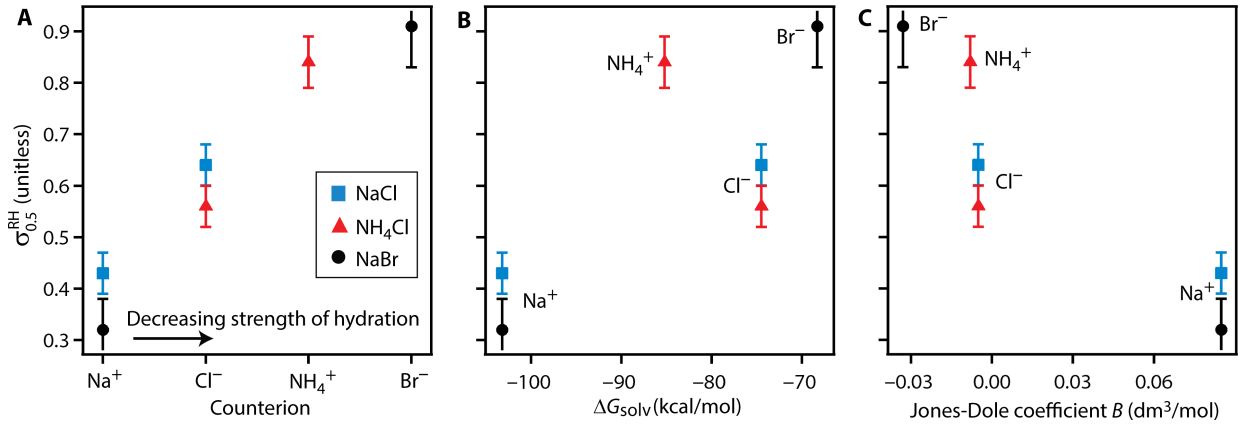


**Fig. 3. Contact efflorescence correlated to trends in ion-specific properties.** (**A**) $\sigma_{0.5}^{RH}$ plotted as a function of the counterion attracted to the PSL CN surface [countercations $Na^+$ and $NH_4^+$ for (−)PSL CN and counteranions $Cl^-$ and $Br^-$ for (+)PSL CN] where the countercations/counteranions are ordered from the most strongly hydrated ($Na^+$/$Cl^-$) to the most weakly hydrated ($NH_4^+$/$Br^-$). (**B** and **C**) $\sigma_{0.5}^{RH}$ plotted as a function of ion-specific hydration properties of the counterion attracted to the PSL CN surface. (B) Gibbs free energy of solvation $\Delta G_{solv}$. (C) Jones-Dole $B$ coefficient. Values for $B$ and $\Delta G_{solv}$ are from the studies of Jenkins and Marcus (*38*) and Kelly *et al.* (*39*), respectively.

assume a stabilizing solute-substrate interaction via, for example, active sites (*24*), epitaxy (*7*), or templating (*12*).

The correlations suggested in Fig. 3 may stem from the different length scales of the competing interactions. Electrostatic interactions can dominate at long ranges (for example, the distance across several water molecules, ~1 nm), whereas hydration-mediated forces can become more important at a short range (*19*, *25*). Any charged functional group on the PSL surface may thus be influencing the orientation of the aqueous ions even before the collision. However, immediately upon contact, ion-surface separation distances are small because of the relatively low concentration of water molecules in a supersaturated aqueous droplet; for example, there are about six water molecules per NaCl ion pair at 60% RH (*26*), which is only enough to fully fill the first solvation shell of the ions (*22*). Penetration of PSL CN into the aqueous droplet requires a cavity to be formed to accommodate the PSL volume and induces the formation of a new interface between the hydrophobic surface and the aqueous phase, a process that requires rearrangement of the water molecules and the ions (*20*, *27*). Because there is insufficient water available in the droplets for changes in water microstructure to occur without disrupting the solvation shell of the ions, it is likely that hydration-mediated forces are influencing the ions closest to the PSL surface (that is, the counterions) at the moment of contact when the initial nonequilibrium PSL-droplet interface forms. Simulations indicate that compression of an ion's solvation shell to form a solvent-shared pair transiently increases the free energy of the ion (*22*). Because it is the free energy difference between the supersaturated solute and crystalline phase that is the driving force for crystal nucleation (*15*, *28*), we speculate that it was this transient increase in free energy that was the additional driving force for efflorescence via collisions with the PSL CN.

## Evidence suggests that destabilizing and transient interactions initiated crystal nucleation

According to classical nucleation theory (CNT), the work necessary for the formation of a crystal nucleus with $n$ molecules of solute is the change in Gibbs free energy ($\Delta G_{nuc}$) associated with the formation of the crystal nucleus, which can be expressed as

$$\Delta G_{nuc} = -n\Delta\mu + \Delta G_{surf} \quad (4)$$

where $\Delta G_{surf}$ is the unfavorable free energy cost of the solid-liquid interface, $\Delta\mu$ is the difference in chemical potential between the metastable aqueous state and the stable crystalline state, and $-n\Delta\mu$ is the favorable decrease in free energy associated with the phase change (*15*, *28*–*30*). [Note that CNT is used here to provide a conceptual basis, but the actual mechanism for NaCl nucleation may be nonclassical, for example, a two-step process, as suggested by simulation (*31*).] The $-n\Delta\mu$ term represents the driving force for nucleation (*30*). $\Delta G_{nuc}$ can be lowered by increasing $\Delta\mu$ or decreasing the contribution of $\Delta G_{surf}$. Simulations have been performed elsewhere that provide trends in free energy as $Na^+$ and $Cl^-$ approach a hydrophobic surface and a carboxyl-terminated surface (*22*, *32*), which are relevant to NaCl collision-induced contact efflorescence with (−)PSL CN. These simulations indicate that the free energy of a $Na^+$ ion increases by ~2 to $3k_BT$ because of the compression of its hydration sphere as it forms a solvent-shared ion pair with a charged carboxyl group (*22*). A transient increase in free energy for a single ion would decrease $\Delta G_{nuc}$ by that same amount through the $-n\Delta\mu$ term in Eq. 4. A free energy increase of ~$2k_BT$ would thus be sufficient to overcome the nucleation barrier if enough $Na^+$ ions [for example, ~200 ions, circa the number in a NaCl crystal nucleus (*31*)] experienced this increase (see Supplementary Text for additional details).

A destabilizing hydration-mediated effect on crystal nucleation would be transient because the ions will only remain in a high-energy state until an equilibrium water activity is established via uptake of additional water molecules to fully hydrate the PSL surface, a process that will occur on microsecond time scales (*33*), which is long relative to the time scale necessary for crystal nucleation (see Supplementary Text) (*15*). Crystal nucleation would thus be expected to occur shortly after the initial moment of contact. As shown in Fig. 4, bright-field images captured during contact efflorescence demonstrate that crystal growth proceeds from the droplet surface, indicative of crystal nucleation initiated at or near the initial point of contact. Furthermore, as demonstrated in fig. S4, contact efflorescence–deliquescence–internally mixed efflorescence cycles of several NaCl particles confirmed that external contact is necessary for crystallization at the high RH observed in our experiments and that the effect is transient, further suggesting that crystal nucleation is induced at the short-lived nonequilibrium CN-droplet interface.

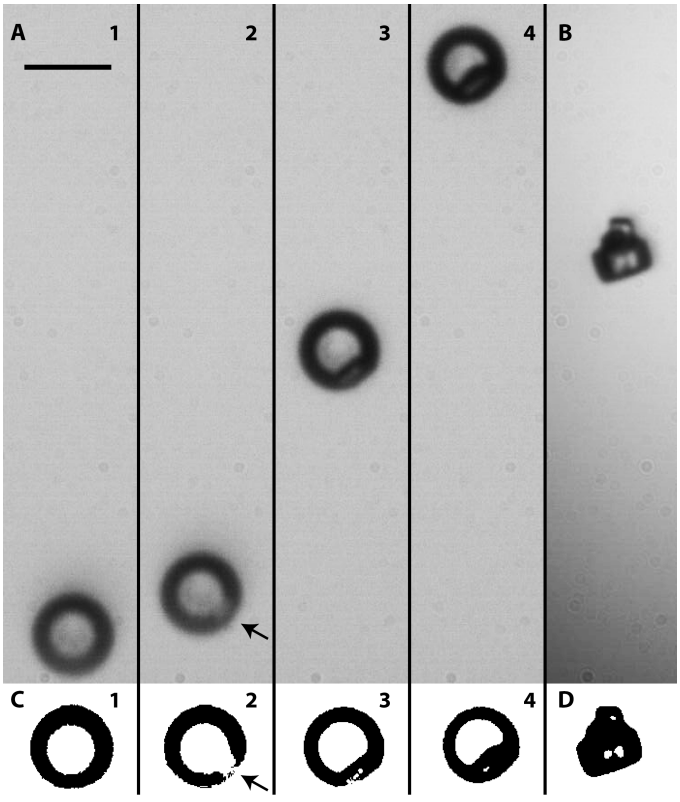


**Fig. 4. Bright-field imaging of collision-induced contact efflorescence.** Crystal nucleation and growth of NaCl following contact with 400-nm (−)PSL CN at 57 ± 1% RH. Scale bar, 10 μm. (**A**) Frame 1 shows the aqueous droplet before contact. The droplet was deliberately positioned at the bottom of the frame to capture the crystal growth process as the droplet moved upward because of loss of water mass. Frame 2 shows the droplet ~20 ms after contact. Crystal growth is apparent near the droplet surface (where indicated by the arrow). Frames 3 and 4, ~90 and 180 ms after contact, respectively, show the progressive growth process. At this RH, complete NaCl efflorescence occurs at ~1 s. This particular particle did not stay trapped after contact efflorescence. (**B**) A fully effloresced NaCl crystal that remained trapped after contact efflorescence. (**C** and **D**) Binary contrast images of the particle shown in each frame of (A) and (B).

## DISCUSSION

Here, we presented evidence for a crystal nucleation pathway in which a transient increase in interfacial free energy induces efflorescence as an ion is forced into close proximity with a charged/hydrophobic surface, which could account for our observed ionic specificity of contact efflorescence. For example, because $NH_4^+$ and $Br^-$ more readily approach a hydrophobic PSL surface than $Na^+$ and $Cl^-$ (*20*, *21*), the transient increase in free energy associated with a collision would be lower for $NH_4^+$ and $Br^-$ counterions than for $Na^+$ and $Cl^-$, consistent with the lower $RH_{0.5}^{CE}$ values observed when $NH_4^+$ and $Br^-$ were the counterions. Notably, for the systems studied here, we see no evidence that the presence of a three-phase interface alone initiates efflorescence at a significantly elevated RH, as evident by the null effect of internally mixed PSLs, which is in contrast to conclusions drawn in regard to contact freezing (*34*). Rather, our observations suggest that movement of the aqueous phase along the three-phase interface (as a result of the collision) is necessary to account for the elevated contact efflorescence RH values. The ion specificity and necessity of a collision for contact efflorescence suggest that rather than stabilizing the crystalline phase, the PSL CN facilitated heterogeneous crystal nucleation by destabilizing the aqueous phase. The NaCl contact efflorescence RH with PSL CN was comparable to or greater than that with soluble crystalline inorganic CN, as observed in our previous study, which correlated contact efflorescence RH to stabilizing solute-substrate interactions (epitaxy) (*7*). For example, the single-collision ($P_{eff}$ = 1) NaCl contact efflorescence RH with (−)PSL CN was 62 ± 1% RH, which is similar to that with $KCl_{(s)}$ CN (64 ± 3% RH) (*7*). This suggests that when considering efflorescence probability, the effect of the transient destabilizing interactions proposed here may, in some cases, rival that of stabilizing solute-substrate interactions.

These observations are consistent with crystal nucleation behavior that has been attributed to nonclassical pathways, such as the two-step mechanism (*14*). The CN used in the present study were of atmospherically relevant sizes. Thus, this report supports the potential atmospheric relevance of nonclassical as well as ion-specific crystal nucleation pathways. Although PSL CN are not directly relevant to the atmosphere, there are a range of insoluble amorphous aerosols found in the atmosphere, both hydrophobic and hydrophilic (*16*, *17*). For example, soot particles are hydrophobic when freshly emitted and, because of surface oxidation during formation and atmospheric processing, can have surface functionality similar to carboxyl (−)PSLs (*35*). Collisions with soot may thus influence the phase state of, for example, sea spray aerosol. However, the extent to which contact efflorescence may influence the phase state of atmospheric aerosols remains uncertain with multiple open questions. It is unclear whether a purely hydrophobic aerosol (that is, without charged functional groups) would induce efflorescence via a collision. Furthermore, any potential aqueous-phase size and temperature dependence on contact efflorescence remains to be explored further, although the efflorescence RH of aqueous aerosols remains markedly similar across a wide range of diameters (*29*) and temperatures (*36*). Also, we note that crystal nucleation and ionic surface propensity have been intensely debated subjects for the past century, and their respective mechanisms remain controversial (*13*, *20*). Thus, the underlying mechanism behind our observations of collision-induced contact efflorescence remains open to speculation, but it is clear from this study that far more particle-particle interactions may influence the phase state of atmospheric aerosols than previously considered, and this points toward a need for an additional theoretical framework for crystal nucleation applied to atmospherically relevant aerosols.

## MATERIALS AND METHODS

### Materials

Surfactant-free PSLs were obtained from Life Technologies. The properties of the PSLs are given in table S1. NaCl (Fisher Scientific; Certified ACS, ≥99.0% purity), $NH_4Cl$ (Sigma-Aldrich; ReagentPlus, ≥99.5% purity), and NaBr (Sigma-Aldrich; ReagentPlus, ≥99% purity) were used without further purification. All aqueous solutions and PSL suspensions were prepared/diluted with filtered high-performance liquid chromatography (HPLC)–grade water (Fisher Scientific) that was filtered before use with a sterile syringe equipped with a filter (pore size, 0.2 μm).

Droplets were generated using a piezo-driven droplet generator with a 15-μm orifice (MicroFab) and then horizontally guided into the trapping region at the center of the flow tube. For homogeneous and contact efflorescence, the stock solution from which droplets were generated was a 5 weight % (wt %) solution of NaCl, NaBr, or $NH_4Cl$.

The inorganic solutions were added to the droplet generator with a syringe equipped with a 0.2-μm filter.

For efflorescence experiments with internally mixed PSLs, the stock PSL/inorganic suspension was 5 wt % NaCl, NaBr, or $NH_4Cl$ and 0.003 wt % PSLs, corresponding to four to five PSLs on average in the droplets once trapped. The PSL/inorganic suspension was made by diluting the stock PSL suspension with filtered inorganic solution (0.2-μm filter). The PSL/inorganic suspension was then added to the droplet generator using a syringe without additional filtration.

### Levitation

The entire experimental arrangement is shown in fig. S1. The optical trap and trapping procedure have been described in detail elsewhere (*7*, *23*). In brief, aqueous droplets were optically levitated in a black-anodized aluminum flow tube [12 mm (inner diameter) × 110 mm (length)] with four window ports. Droplets were levitated with two vertical counterpropagating beams generated using the output of individual continuous-wave diode-pumped neodymium-doped yttrium aluminium garnet lasers (wavelength $\lambda = 532$ nm). A Bessel beam was generated from an axicon and focused onto the droplet from above. A Gaussian beam was focused from below. The reproducibility of the size of levitated droplets in this experimental setup has been established (*7*, *23*), and droplets used in the present study were 10 ± 2 μm in diameter.

### PSL CN preparation

PSL CN were wet-generated from a dilute PSL suspension using a medical nebulizer (Omron NE-U22). The dilute PSL suspension was made with three drops (~150 μl) of the stock 400-nm PSL suspension or six drops (~300 μl) of the stock 800-nm PSL suspension diluted with 2 ml of filtered HPLC-grade water (0.2-μm filter pore size). The dilute PSL suspension was used immediately and discarded after each day of experiments. A fresh suspension was made daily. The pH of the suspensions was ~6. To minimize interference from other aqueous electrolytes, the suspensions were not buffered, and the pH was not adjusted. Only filtered HPLC-grade water was added to the PSL suspension. The PSL surface charges were not known before contact (that is, after nebulization/drying).

### Aerosol flow and RH control

A $N_2$ gas flow was used to control the RH and deliver the PSL CN into the flow tube. PSL CN were wet-generated from the diluted PSL solution using a medical nebulizer and then dried in a diffusion drier. The dry $N_2$ gas flow carrying the CN was mixed with the $N_2$ gas flow that was humidified with a water bubbler. The mixed gas flow with the CN entered the flow tube from the bottom. Calibrated RH probes were placed immediately before and after the flow tube. For each individual experiment, the RH within the flow cell was determined as the mean readout from the two calibrated RH probes (±1 SD). The RH typically varied by <0.5% over the 5-min residence time of an experiment.

### Imaging and determining collision number

The imaging techniques used here are discussed extensively in our previous publications and many additional examples can be found therein (*7*, *23*). Phase transformations and PSL-droplet collisions were monitored by imaging scattered laser light using a custom LabVIEW image acquisition and postprocessing program (*23*). Near-field 632.8-nm scattered laser light was collected with a microscope objective and a complementary metal-oxide semiconductor camera [frame area of interest (AOI) size, 140 pixels × 720 pixels; frame rate, ~150 frames/s (fps)]. A band-pass filter transmitted the 632.8-nm light and removed the 532-nm light from the trapping lasers. Examples of using the 632.8-nm near-field scatter to monitor collisions are shown in movies S1 (contact without efflorescence) and S2 (contact efflorescence). Far-field elastically scattered 532-nm laser light was collected with a separate microscope objective and polarization filter and imaged using a charge-coupled device camera (frame AOI size, 300 pixels × 1280 pixels; frame rate, ~25 fps). When imaged in the far field, the 532-nm elastically scattered light from a levitated droplet contained linear interference fringes. The angular distribution and intensity of these fringes describe a particle's phase function, which is dependent on the size of the particle (*7*, *23*). The far-field images were used to detect phase transformations, confirm the PSL CN size, and monitor collisions, as demonstrated in fig. S2 and movies S3 and S4. For internally mixed efflorescence experiments, the far-field images also confirmed the presence of internally mixed PSLs, as demonstrated in movie S5.

The number of PSL-droplet collisions was determined with a combined analysis of the far-field and near-field images. In the far field and near field, a collision that induces efflorescence causes an abrupt and distinct change in the appearance of the scattered laser light. However, not every collision induced efflorescence. In the near field, the occurrence of a PSL-droplet collision was evident by the PSL trajectory, and the scavenging of the PSL by the droplet resulted in the disappearance of the PSL laser scatter. As seen in movie S1, if efflorescence did not occur, the presence of the PSLs was still evident at the droplet surface. In the far field, the occurrence of a collision without efflorescence was unambiguous because of the insoluble nature of the PSL and the difference in the refractive index between the PSL and the aqueous phase, which resulted in disruptions in the linear interference fringes of the aqueous droplet (movie S3). Thus, a collision that was indicated in the near field was confirmed by changes in the far-field laser scatter pattern (*23*).

The far-field image analysis used to detect efflorescence and confirm the occurrence of collisions was developed previously (*23*) and described in brief here. For the optical orientation used in this study, far-field images of liquid droplets were symmetric around a vertically centered line, and the linear interference fringes appeared horizontally uniform. For a liquid droplet with an immersed PSL, the scatter was distorted by the differing refractive indices of the PSL and the aqueous phase. For a crystalline particle, the scatter was asymmetric and not uniformly distributed. The different scatter patterns were distinguished by their level of asymmetry. To quantitatively determine the asymmetry in the far-field images, a template-based autocorrelation of the far-field images was used. In this image analysis, the template image was the original image offset in the horizontal ($x$) direction (that is, parallel to the direction of the linear interference fringes). An image within a recorded sequence was duplicated and then offset horizontally using an offset of $x = 10$. A "defect image" was generated from the original image and offset duplicate image using the absolute difference of the intensity values of overlapping pixels. For a liquid droplet, the average intensity of the defect image was low, as shown in fig. S2. PSL contact and efflorescence resulted in an increase in defect image intensity. An increase in defect image intensity and an upward movement of the particle due to loss of water mass were unambiguous indicators of efflorescence. A smaller increase in defect image intensity and no upward movement indicated contact without efflorescence.

### Contact efflorescence experimental sequence

All experiments were performed at room temperature (295 ± 1 K). The RH in the flow cell was established at a constant value with a variation of <±0.5% RH throughout the experiment. A droplet was then trapped, and the PSL CN were nebulized briefly (~2 s). The time between nebulization of CN and their appearance in the levitation chamber was ~2 min. PSL-droplet collisions were monitored until either contact efflorescence occurred, the maximum residence time of 5 min was reached, or ~10 collisions were observed. The near-field and far-field images were postprocessed to verify the number of collisions.

### Statistical analysis

For the RH bins shown in Fig. 2 (A to C) (see tables S2 to S5), the median RH is reported with uncertainty given by the upper and lower quartiles of the ensemble of individual RH measurements with propagated uncertainty from the individual measurements (1 SD). For an RH bin containing an ensemble of $N_{tot}$ droplets, the relative error (1σ level) in $N_{eff}/N_{tot}$ ($P_{hom}$ and $P_{IM}$; Eq. 1) was taken as $1/\sqrt{N_{tot}}$, and for $P_{CE}$, the uncertainty was calculated as $1/\sqrt{N_{col}}$ (*37*). $P_{hom}$, $P_{IM}$, and $P_{CE}$ are reported in Fig. 2 (A to C) with error bars of $\pm 1/\sqrt{N_{tot}}$ and $\pm 1/\sqrt{N_{col}}$, respectively. The homogeneous and internally mixed efflorescence RH, where $P_{hom}$ and $P_{IM} = 0.5$ ($RH_{0.5}^{hom}$ and $RH_{0.5}^{IM}$, respectively), and the collision-induced contact efflorescence RH, where $P_{CE} = 0.5$ ($RH_{0.5}^{CE}$), were taken as the median efflorescence RH values (*8*). If the available data points did not yield an RH bin where $P = 0.5$, then the $RH_{0.5}$ value was extrapolated between the highest RH bin, where $P > 0.5$, and the lowest RH bin, where $P < 0.5$. Uncertainty in $\sigma_{0.5}^{RH}$ (Eq. 3) was propagated at a 1σ level from the uncertainty in $RH_{0.5}^{CE}$ and $RH_{0.5}^{hom}$.

## SUPPLEMENTARY MATERIALS

Supplementary material for this article is available at http://advances.sciencemag.org/cgi/content/full/3/7/e1700425/DC1

Supplementary Text
fig. S1. The experimental setup used for efflorescence experiments.
fig. S2. Image processing to detect collisions and efflorescence.
fig. S3. Bright-field images of a droplet with internally mixed PSLs.
fig. S4. Contact efflorescence–deliquescence–internally mixed efflorescence cycle.
table S1. Manufacturer-stated properties of the PSL CN.
table S2. Homogeneous and internally mixed efflorescence results.
table S3. NaCl contact efflorescence results for individual trials.
table S4. $NH_4Cl$ contact efflorescence results for individual trials.
table S5. NaBr contact efflorescence results for individual trials.
movie S1. Near-field tracking of CN-droplet collisions without efflorescence.
movie S2. Near-field tracking of a CN-droplet collision resulting in efflorescence.
movie S3. Far-field tracking of CN-droplet collisions without efflorescence.
movie S4. Far-field tracking of a CN-droplet collision resulting in efflorescence.
movie S5. Far-field imaging of a droplet with internally mixed PSLs.
References (*40*–*44*)

## REFERENCES AND NOTES


1. S. T. Martin, Phase transitions of aqueous atmospheric particles. *Chem. Rev.* **100**, 3403–3454 (2000).
2. S. P. Hersey, J. S. Craven, A. R. Metcalf, J. Lin, T. Lathem, K. J. Suski, J. F. Cahill, H. T. Duong, A. Sorooshian, H. H. Jonsson, M. Shiraiwa, A. Zeund, A. Nenes, K. A. Prather, R. C. Flagan, J. H. Seinfeld, Composition and hygroscopicity of the Los Angeles Aerosol: CalNex. *J. Geophys. Res. Atmos.* **118**, 3016–3036 (2013).
3. D. Tobias, A. Stern, M. D. Baer, Y. Levin, C. J. Mundy, Simulation and theory of ions at atmospherically relevant aqueous liquid-air interfaces. *Annu. Rev. Phys. Chem.* **64**, 339–359 (2013).
4. W. Hua, D. Verreault, Z. Huang, E. M. Adams, H. C. Allen, Cation effects on interfacial water organization of aqueous chloride solutions. I. Monovalent cations: $Li^+$, $Na^+$, $K^+$, and $NH_4^+$. *J. Phys. Chem. B* **118**, 8433–8440 (2014).
5. S. Ghosal, J. C. Hemminger, H. Bluhm, B. S. Mun, E. L. D. Hebenstreit, G. Ketteler, D. F. Ogletree, F. G. Requejo, M. Salmeron, Electron spectroscopy of aqueous solution interfaces reveals surface enhancement of halides. *Science* **307**, 563–566 (2005).
6. C. Pöhlker, J. Saturno, M. Krüger, J.-D. Förster, M. Weigand, K. T. Wiedemann, M. Bechtel, P. Artaxo, M. Andreae, Efflorescence upon humidification? X-ray microspectroscopic in situ observation of changes in aerosol microstructure and phase state upon hydration. *Geophys. Res. Lett.* **41**, 3681–3689 (2014).
7. R. D. Davis, S. Lance, J. A. Gordon, S. B. Ushijima, M. A. Tolbert, Contact efflorescence as a pathway for crystallization of atmospherically relevant particles. *Proc. Natl. Acad. Sci. U.S.A.* **112**, 15815–15820 (2015).
8. A. Pant, M. T. Parsons, A. K. Bertram, Crystallization of aqueous ammonium sulfate particles internally mixed with soot and kaolinite: Crystallization relative humidities and nucleation rates. *J. Phys. Chem. A* **110**, 8701–8709 (2006).
9. A. Even, H. M. Tem Brink, A. Khlystov, A. Smekens, P. Berghmans, R. Van Grieken, The influence of black carbon on the crystallization point of salt aerosol. *J. Aerosol Sci.* **31**, 336–337 (2000).
10. A. R. Ravishankara, Heterogeneous and multiphase chemistry in the troposphere. *Science* **276**, 1058–1065 (1997).
11. R. R. Dickerson, S. Kondragunta, G. Stenchikov, K. L. Civerolo, B. G. Doddridge, B. N. Holben, The impact of aerosols on solar ultraviolet radiation and photochemical smog. *Science* **278**, 827–830 (1997).
12. L. M. Hamm, A. J. Giuffre, N. Han, J. Tao, D. Wang, J. J. De Yoreo, P. M. Dove, Reconciling disparate views of template-directed nucleation through measurement of calcite nucleation kinetics and binding energies. *Proc. Natl. Acad. Sci. U.S.A.* **111**, 1304–1309 (2014).
13. J. J. De Yoreo, P. U. P. A. Gilbert, N. A. J. M. Sommerdijk, R. L. Penn, S. Whitelam, D. Joester, H. Zhang, J. D. Rimer, A. Navrotsky, J. F. Banfield, A. F. Wallace, F. M. Michel, F. C. Meldrum, H. Cölfen, P. M. Dove, Crystallization by particle attachment in synthetic, biogenic, and geologic environments. *Science* **349**, aaa6760 (2015).
14. R. Grossier, Z. Hammadi, R. Morin, S. Veesler, Predictive nucleation of crystals in small volumes and its consequences. *Phys. Rev. Lett.* **107**, 025504 (2011).
15. J. Niehaus, W. Cantrell, Contact freezing of water by salts. *J. Phys. Chem. Lett.* **6**, 3490–3495 (2015).
16. M. C. Facchini, M. Rinaldi, S. Decesari, C. Carbone, E. Finessi, M. Mircea, S. Fuzzi, D. Ceburnis, R. Flanagan, E. D. Nilsson, G. de Leeuw, M. Martino, J. Woeltjen, C. D. O'Dowd, Primary submicron marine aerosol dominated by insoluble organic colloids and aggregates. *Geophys. Res. Lett.* **35**, L17814 (2008).
17. K. Adachi, P. R. Buseck, Changes of ns-soot mixing states and shapes in an urban area during CalNex. *J. Geophys. Res. Atmos.* **118**, 3723–3730 (2013).
18. N. Riemer, M. West, R. A. Zaveri, R. C. Easter, Simulating the evolution of soot mixing state with a particle-resolved aerosol model. *J. Geophys. Res. Atmos.* **114**, D09202 (2009).
19. Z. He, W. J. Xie, Z. Liu, G. Liu, Z. Wang, Y. Q. Gao, J. Wang, Tuning ice nucleation with counterions on polyelectrolyte brush surfaces. *Sci. Adv.* **2**, e1600345 (2016).
20. T. López-León, M. J. Santander-Ortega, J. Ortega-Vinuesa, D. Bastos-González, Hofmeister effects in colloidal systems: Influence of the surface nature. *J. Phys. Chem. C* **112**, 16060–16069 (2008).
21. T. Oncsik, G. Trefalt, M. Borkovec, I. Szilagyi, Specific ion effects on particle aggregation induced by monovalent salts within the Hofmeister series. *Langmuir* **31**, 3799–3807 (2015).
22. N. Schwierz, D. Horinek, R. R. Netz, Specific ion binding to carboxylic surface groups and the pH dependence of the Hofmeister series. *Langmuir* **31**, 215–225 (2015).
23. R. D. Davis, S. Lance, J. A. Gordon, M. A. Tolbert, Long working-distance optical trap for in situ analysis of contact-induced phase transformations. *Anal. Chem.* **87**, 6186–6194 (2015).
24. L. Ladino, O. Stetzer, F. Lüönd, A. Welti, U. Lohmann, Contact freezing experiments of kaolinite particles with cloud droplets. *J. Geophys. Res.* **116**, D22202 (2011).
25. T. T. Duignan, D. F. Parsons, B. W. Ninham, A continuum solvent model of ion–ion interactions in water. *Phys. Chem. Chem. Phys.* **16**, 22014–22027 (2014).
26. A. S. Wexler, S. L. Clegg, Atmospheric aerosol models for systems including the ions $H^+$, $NH_4^+$, $Na^+$, $SO_4^{2-}$, $NO_3^-$, $Cl^-$, $Br^-$, and $H_2O$. *J. Geophys. Res. Atmos.* **107**, ACH 14-1–ACH 14-14 (2002).
27. D. Chandler, Interfaces and the driving force of hydrophobic assembly. *Nature* **437**, 640–647 (2005).
28. N. Fukuta, A study of the mechanism of contact ice nucleation. *J. Atmos. Sci.* **32**, 1597–1603 (1975).
29. Y. Gao, L. E. Yu, S. B. Chen, Efflorescence relative humidity of mixed sodium chloride and sodium sulfate particles. *J. Phys. Chem. A* **111**, 10660–10666 (2007).
30. V. I. Kalikmanov, *Nucleation Theory* (Springer, 2013), vol. 860.
31. D. Chakraborty, G. N. Patey, Evidence that crystal nucleation in aqueous NaCl solution occurs by the two-step mechanism. *Chem. Phys. Lett.* **587**, 25–29 (2013).
32. N. Schwierz, D. Horinek, R. R. Netz, Anionic and cationic Hofmeister effects on hydrophobic and hydrophilic surfaces. *Langmuir* **29**, 2602–2614 (2013).
33. D. Lamb, J. Verlinde, *Physics and Chemistry of Clouds* (Cambridge Univ. Press, 2011).

34. R. P. Sear, Nucleation at contact lines where fluid-fluid interfaces meet solid surfaces. *J. Phys. Condens. Matter* **19**, 466106 (2007).
35. J.-O. Müller, D. S. Su, U. Wild, R. Schlögl, Bulk and surface structural investigations of diesel engine soot and carbon black. *Phys. Chem. Chem. Phys.* **9**, 4018–4025 (2007).
36. T. B. Onasch, R. L. Siefert, S. D. Brooks, A. J. Prenni, B. Murray, M. A. Wilson, M. A. Tolbert, Infrared spectroscopic study of the deliquescence and efflorescence of ammonium sulfate aerosol as a function of temperature. *J. Geophys. Res. Atmos.* **104**, 21317–21326 (1999).
37. N. Hoffmann, D. Duft, A. Kiselev, T. Leisner, Contact freezing efficiency of mineral dust aerosols studied in an electrodynamic balance: Quantitative size and temperature dependence for illite particles. *Faraday Discuss.* **165**, 383–390 (2013).
38. H. D. B. Jenkins, Y. Marcus, Viscosity B-coefficients of ions in solution. *Chem. Rev.* **95**, 2695–2724 (1995).
39. C. P. Kelly, C. J. Cramer, D. G. Truhlar, Aqueous solvation free energies of ions and ion–water clusters based on an accurate value for the absolute aqueous solvation free energy of the proton. *J. Phys. Chem. B* **110**, 16066–16081 (2006).
40. M. Elzbieciak-Wodka, M. Popescu, F. J. Montes Ruiz-Cabello, G. Trefalt, P. Maroni, M. Borkovec, Measurements of dispersion forces between colloidal latex particles with the atomic force microscope and comparison with Lifshitz theory. *J. Chem. Phys.* **140**, 104906 (2014).
41. F. J. Montes Ruiz-Cabello, G. Trefalt, T. Oncsik, I. Szilagyi, P. Maroni, M. Borkovec, Interaction forces and aggregation rates of colloidal latex particles in the presence of monovalent counterions. *J. Phys. Chem. B* **119**, 8184–8193 (2015).
42. C. Kidd, V. Perraud, B. J. Finlayson-Pitts, Surfactant-free latex spheres for size calibration of mobility particle sizers in atmospheric aerosol applications. *Atmos. Environ.* **82**, 56–59 (2014).
43. R. E. H. Miles, S. Rudić, A. J. Orr-Ewing, J. P. Reid, Sources of error and uncertainty in the use of cavity ring down spectroscopy to measure aerosol optical properties. *Aerosol Sci. Tech.* **45**, 1360–1375 (2011).
44. J. Smith, K. C. Barsanti, H. R. Friedli, M. Ehn, M. Kulmala, D. R. Collins, J. H. Scheckman, B. J. Williams, P. H. McMurry, Observations of aminium salts in atmospheric nanoparticles and possible climatic implications. *Proc. Natl. Acad. Sci. U.S.A.* **107**, 6634–6639 (2010).

**Acknowledgments**

**Funding:** This work was funded by the NSF (grant AGS1506691) and a NASA Earth and Space Science Fellowship (NNX13AN69H). **Author contributions:** R.D.D. designed the research, performed the experiments, analyzed the data, and wrote the manuscript. M.A.T. supervised the project and discussed the results and writing of the manuscript. **Competing interests:** The authors declare that they have no competing interests. **Data and materials availability:** All data needed to evaluate the conclusions in the paper are present in the paper and/or the Supplementary Materials. Additional data related to this paper may be requested from the authors.

Submitted 8 February 2017
Accepted 15 June 2017
Published 19 July 2017
10.1126/sciadv.1700425

**Citation:** R. D. Davis, M. A. Tolbert, Crystal nucleation initiated by transient ion-surface interactions at aerosol interfaces. *Sci. Adv.* **3**, e1700425 (2017).